Geochimica et Cosmochimica Acta, Vol. 68, No. 23, pp. 4799–4808, 2004

0016-7037/04 $30.00 + .00

ELSEVIER

doi:10.1016/j.gca.2004.05.031

Site-specific incorporation of uranyl carbonate species at the calcite surface

RICHARD J. REEDER,[1,*] EVERT J. ELZINGA,[1] C. DREW TAIT,[2] K. D. RECTOR,[3] ROBERT J. DONOHOE,[3] and DAVID E. MORRIS[2]

[1]Department of Geosciences and Center for Environmental Molecular Science, State University of New York at Stony Brook, Stony Brook, NY 11794-2100, USA

[2]Chemistry Division, G. T. Seaborg Institute for Transactinium Science, Los Alamos National Laboratory, Los Alamos, NM 87545, USA

[3]Biosciences Division, G. T. Seaborg Institute for Transactinium Science, Los Alamos National Laboratory, Los Alamos, NM 87545, USA

(*Received January* 29, 2004; *accepted in revised form May* 17, 2004)

Abstract—Spatially resolved luminescence spectra from U(VI) co-precipitated at the $(10\bar{1}4)$ growth surface of synthetic calcite single crystals confirm heterogeneous incorporation corresponding to the distribution of structurally non-equivalent steps composing the vicinal surfaces of spiral growth hillocks. Spectral structure from U(VI) luminescence at the "–" vicinal regions and featureless, weak luminescence at the "+" vicinal regions are consistent with previously reported observations of enrichment at the former sites during calcite growth. Luminescence spectra differ between the non-equivalent regions of the crystal, with the spectral features from the "–" vicinal region corresponding to those observed in bulk calcite samples. Subtle spectral shifts are observed from U(VI) co-precipitated with microcrystalline calcite synthesized by a different method, and all of the U(VI)-calcite sample spectra differ significantly from that of U(VI) co-precipitated with aragonite.

The step-selective incorporation of U(VI) can be explained by a proposed model in which the allowed orientation for adsorption of the dominant calcium uranyl triscarbonate species is controlled by the atomic arrangement at step edges. Differences in the tilt angles of carbonate groups between non-equivalent growth steps favor adsorption of the calcium uranyl triscarbonate species at "–" steps, as observed in experiments.

1. INTRODUCTION

Where multiple attachment sites are present at a solid surface, binding preferences may result in heterogeneous sorption and incorporation of trace species in solution, including radionuclides and other contaminants. If preferences for binding at different sites contrast greatly, the overall interaction of a dissolved species with the surface may depend strongly on the distribution and availability of favored sites, and consequently may lead to either enhanced or diminished uptake capacity. If the distinct sites are spatially segregated at the surface, uptake preferences may become discernible, and their study may provide insight to molecular models of metal interactions at the solid-water interface.

Heterogeneous incorporation of trace U(VI) species has been observed at the $(10\bar{1}4)$ surface of calcite ($CaCO_3$) (Reeder et al., 2001), the most common growth form as well as the perfect cleavage. Unlike the heterogeneous interactions between contrasting edge and basal-plane sites of clay minerals, the source of the differential incorporation for calcite has been associated with the presence of distinct sites within structurally non-equivalent growth steps on a single face but differing in their orientation. With growth, differential incorporation between the non-equivalent steps produces regions within the crystal enriched and depleted in U (Reeder et al., 2001). The origin of the different step orientations is a consequence of the spiral growth mechanism, which has been observed to operate over a wide range of calcite supersaturation conditions (cf. Gratz et al., 1993; Paquette and Reeder, 1995; Teng et al., 1999). In contrast to curving, circular step patterns seen on the faces of some crystals, growth steps on the calcite $(10\bar{1}4)$ face tend to parallel two dominant directions, resulting in polygonized spirals, or growth hillocks. Owing to surface symmetry, steps having similar atomic structure at their edges are segregated into the vicinal surfaces composing the flanks of these shallow microtopographic features.

Reeder et al. (2001) used synchrotron micro X-ray fluorescence mapping to demonstrate that the U(VI) distribution on a calcite single crystal surface grown from a U(VI)-containing solution is strongly enriched on one pair of vicinal surfaces relative to the other, indicating that these steps favor U(VI) incorporation. Although uranium concentrations observed in the calcite depend on its concentration in the growth solution, the magnitude of this differential uptake was typically a factor of 2 to 6. This step-selective, differential incorporation effectively yields different solution-solid partition coefficients for U(VI) co-precipitation at different vicinal regions on calcite and demonstrates that trace element partitioning is influenced by the energetic and possibly mechanistic differences associated with attachment at different surface sites.

Similar step-selective uptake behavior is known for incorporation of divalent metals and several oxyanions at the calcite $(10\bar{1}4)$ surface (e.g., Paquette and Reeder, 1995; Reeder, 1996; Elzinga and Reeder, 2002). For divalent metals, which substitute in the Ca site, a correlation between step preference and the structure of adsorbed surface complexes has been proposed (Elzinga and Reeder, 2002). No explanations have been proposed to account for the differential uptake of U(VI) at the calcite surface.

Our goal in the present paper is two-fold. We report new observations from spatially resolved luminescence spectroscopy for the non-equivalent vicinal regions of U(VI)-contain-

* Author to whom correspondence should be addressed (rjreeder@stonybrook.edu).

ing calcite single crystals that support the heterogeneous incorporation and suggest differences not previously recognized. We also present a model to explain the preferential incorporation of uranyl carbonate species at the steps observed to be favored.

2. PREVIOUS STUDIES

Several studies have examined spiral growth on the calcite ($10\bar{1}4$) face and its relationship to metal uptake (e.g., Gratz et al., 1993; Staudt et al., 1994; Paquette and Reeder, 1995; Reeder, 1996; Teng et al., 1999; Davis et al., 2000). Over a wide range of supersaturation conditions, growth spirals are observed to exhibit a polygonized geometry governed by the advance of predominantly straight step segments parallel to the symmetrically equivalent [$44\bar{1}$] and [$48\bar{1}$] directions (Fig. 1). Paquette and Reeder (1995) noted that the *c*-glide is the only symmetry element of the bulk structure that is normal to the ($10\bar{1}4$) face and effectively operates as a mirror symmetry element on a surface containing arrays of steps. Although the *c*-glide symmetrically relates the [$44\bar{1}$] and [$48\bar{1}$] directions, step edges parallel to either orientation but moving in opposite directions are not symmetrically related. Consequently, two pairs of equivalent vicinal faces typically compose the growth spirals, but these pairs are non-equivalent (Fig. 1). Equivalent steps and vicinal surfaces have been denoted by "+" or "–." Staudt et al. (1994) and Paquette and Reeder (1995) have described the structural differences that distinguish the steps and the kink sites within them.

Individual calcite crystals are composed of multiple growth sectors, each exhibiting a heterogeneous distribution pattern associated with growth spirals on the corresponding {$10\bar{1}4$}-type faces. Consequently, spectroscopic methods applied to bulk samples (i.e., entire crystals or multiple crystals ground into powder form) average over all uranium incorporated at both the + and – vicinal regions. Such bulk information is valuable, but it may not necessarily reveal differences in the uranium residing in the distinct regions associated with the non-equivalent vicinals.

In a previous study, we used extended X-ray absorption fine-structure (EXAFS) and luminescence spectroscopies to characterize U(VI) species incorporated into both single crystals and polycrystals of calcite (Reeder et al., 2001). Results obtained for luminescence decay kinetics for bulk powdered samples of single crystals at 77 K revealed the presence of at least two uranyl species in the bulk crystal, as demonstrated by two exponentials with lifetimes 264 ± 15 and 98 ± 7 μs. Gated luminescence spectra obtained for these long and short lifetime populations were found to correspond to (1) a triscarbonate-like species and (2) a spectrally red-shifted species interpreted by Reeder et al. (2000) to have an equatorial coordination of five oxygens. EXAFS spectra obtained from crushed and ground samples of the single crystals were fit with two axial oxygens at 1.80 ± 0.01 Å, five to six equatorial oxygens at 2.36 ± 0.02 Å, and approximately three carbons at 2.92 ± 0.02 Å. The equatorial oxygen shell, however, was equally well fit with a split oxygen shell with path lengths at 2.28 and 2.43 Å, which was consistent with (although not uniquely diagnostic of) multiple uranyl species.

In view of the evidence that more than one uranyl species exists in the calcite single crystals, we considered it possible, even likely, that their origin could be attributed to incorporation at non-equivalent growth steps. Because these steps present distinct coordination, they could induce subtle differences in final coordination of incorporated uranyl species. In an effort to identify any such differences, Reeder et al. (2001) examined U L_3 polarized XANES spectra in adjacent, non-equivalent vicinals from several crystals (Fig. 10 in Reeder et al., 2001). A distinct feature observed in the XANES spectra ~10 eV above the absorption maximum has been attributed to multiple scattering in the dioxo unit (Hudson et al., 1995). As this moiety is strongly dichroic, differences in the XANES spectra have been associated with the orientation of the dioxo unit relative to the polarization of the incident synchrotron beam (Hudson et al., 1996). The XANES spectra for the uranyl-containing single crystals failed to show any clear differences for the few orientations examined ($\parallel$ and $\perp$ to the c-axis). However, the failure to identify differences in the XANES spectra does not preclude the existence of different uranyl species incorporated at the non-equivalent steps. Although this previous work identified structural differences between non-equivalent surface steps as the basis for the differential incorporation, no detailed structural model was proposed to account for the observed step preference. In part, this reflected a lack of direct information about the surface complexes of uranyl sorbed at the calcite surface. Because adsorption at steps is expected to precede incorporation, step-selective incorporation may be explained by differences in sorption preferences of the impurity between the steps. In other words, structural differences between steps may lead to favored sorption and subsequent incorporation of impurities at one step relative to the other.

Recently, Elzinga et al. (2004) examined the structure of uranyl carbonate complexes sorbed at the calcite-water interface using EXAFS and luminescence spectroscopies. These in-situ studies examined the local structure of uranyl sorbed to calcite powder from calcite-saturated solutions (pH 7.4–8.3) over a range of total U concentrations. Although the calcite saturation state used in these sorption studies was different from those used in the studies characterizing U(VI) incorporation into single crystals during calcite growth considered here, the solution speciation of U(VI) was similar in both systems. Elzinga et al. (2004) reported that at conditions below saturation with respect to uranyl hydroxides (<500 μmol/L uranium in calcite-saturated solutions of pH 8.3) two uranyl surface complexes are present at the calcite surface. Both species resemble the calcium uranyl triscarbonate-like complex, $Ca_2UO_2(CO_3)_3(aq)$ characterized by Bernhard et al. (1996, 2001), which also dominates the U(VI) speciation in solution in these systems. Subtle differences in the luminescence spectra of these species suggest a difference in interaction with calcite surface sites between both species, leading to (subtle) differences in the coordination of the carbonate groups in the equatorial O shell of sorbed U(VI), and possibly Ca atoms in different positions with respect to the equatorial plane. Due to the similarity in aqueous U(VI) speciation in the sorption study of Elzinga et al. (2004) and the present study, it is likely that U(VI) sorbs to growth step sites as a calcium uranyl triscarbonate species, perhaps in several variants, before incorporation into the calcite lattice during calcite growth.

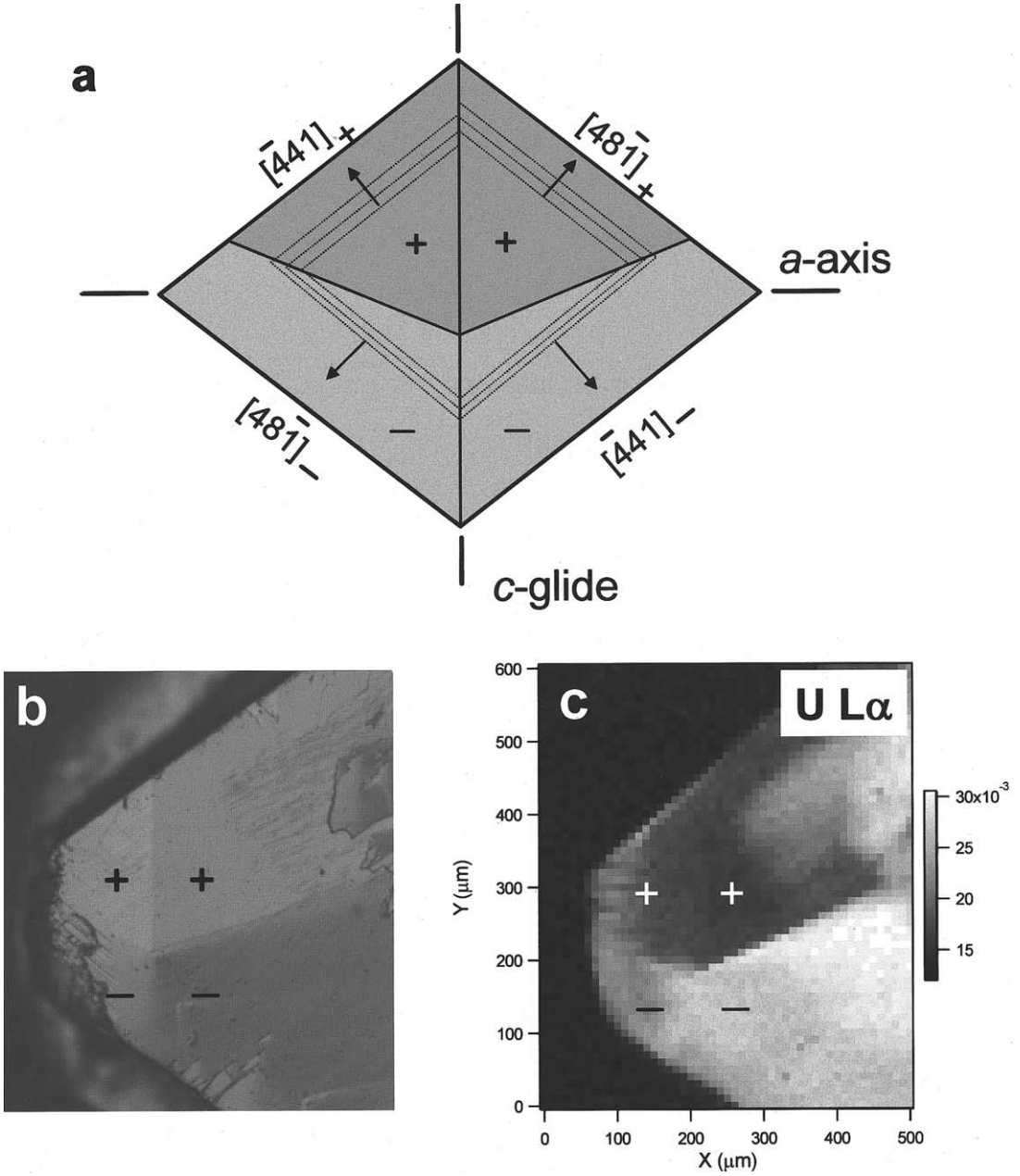

Fig. 1. (a) Schematic of an idealized $(10\bar{1}4)$ growth face showing the disposition of the two pairs of vicinal faces composing a polygonized growth hillock. Vicinal surfaces are distinguished by the orientation of growth steps and their direction of advance during growth. The *c*-glide is perpendicular to the growth face and symmetrically relates growth steps (dashed lines) in the two vicinal faces at top labeled "+" and also in the vicinals at bottom labeled "–." However, steps in + vicinals are not symmetrically equivalent to those in – vicinals. (b) Differential interference contrast image of a portion of an as-grown calcite crystal showing a single growth hillock on a $(10\bar{1}4)$ face. Vicinal surfaces are labeled as shown in (a). (c) A synchrotron μ-XRF map showing the U distribution (as U $L\alpha$ count rate) on the $(10\bar{1}4)$ growth face of the crystal in (b). Uranium is enriched in the – vicinal region (light shading) and depleted in the + vicinal region (dark shading). Modified after Reeder et al. (2001).

3. SAMPLES AND METHODS

3.1. Synthesis of Uranyl-Doped Calcite Samples

The uranyl-containing calcite samples discussed in this paper were prepared during previous studies. Two different co-precipitation methods were used to obtain finely crystalline powders and single crystals of calcite. New luminescence spectroscopic results are reported for single-crystal samples. Although complete details are provided in the original papers, we summarize the methods used for uranyl co-precipitation with calcite here.

3.1.1. Method I: Microcrystalline U(VI)-Doped Calcite

The finely polycrystalline U(VI)-doped calcite samples were taken from the study of Reeder et al. (2001). These were

synthesized using a constant-addition method, in which solutions of $CaCl_2$ and $NaHCO_3$ were delivered at a constant rate using a dual-syringe pump to a stirred reaction vessel through which water-saturated air was bubbled. After an initial period of increasing saturation, the system attained a steady-state calcite growth rate, characterized by constant pH (8.1–8.2), with an estimated saturation index (SI) of 1.4 to 1.5. After the steady state was reached, uranyl was added to give an initial U(VI) concentration of 50 μmol/L, and the $CaCl_2$ syringe was replaced with one also containing a predetermined amount of U(VI) to maintain a constant U(VI) concentration in solution. The growth solutions were undersaturated with respect to schoepite and rutherfordine. The finely polycrystalline calcite product (as confirmed by XRD) was vacuum filtered, washed repeatedly in deionized water, and dried at 50°C. The U concentration in the calcite was determined to be ~725 ppm (Reeder et al., 2001). This co-precipitation technique was referred to as method I in Reeder et al. (2001), and we retain that terminology here.

3.1.2. *Method II: Single-Crystal U(VI)-Doped Calcite*

The calcite single-crystal specimens were also taken from the study of Reeder et al. (2001). The crystals were grown using the modified free-drift procedure described by Paquette and Reeder (1995). Solid $(NH_4)_2CO_3$ was allowed to decompose at room-temperature within a sealed reaction vessel containing a 0.01 mol/L $CaCl_2$ solution. Carbon dioxide gas diffused into the solution, providing a nearly steady-state source of dissolved carbonate (~8 mmol/L total CO_2). The solution pH initially rose to 7.5 to 7.8 and remained nearly constant for periods up to two weeks, with an estimated calcite saturation index of 0.6 to 0.8. After the first appearance of crystals, U(VI) was added to the growth solution to give an initial concentration of 40 μmol/L. Growth was terminated after ~2 weeks, over which time rhomb-shaped calcite single crystals ($\leq$1 mm) formed on vessel walls and substrates provided. This method requires the use of a background electrolyte (NH_4Cl) at an ionic strength of 1.75 mol/L. Final calcite crystals described in this paper were found to contain average U concentrations of 225 ppm, although the U distribution is heterogeneous as described below. This procedure for growing U(VI)-doped calcite single-crystals was referred to as method II in Reeder et al. (2001), and that terminology is used here.

Water-clear single crystals of calcite (method II) were recovered from the substrates after ~13 d, rinsed in deionized water, and allowed to dry. Crystals having visibly flat $(10\bar{1}4)$ faces were selected for differential-interference contrast (DIC) and fluorescence spectroscopy imaging. DIC imaging revealed the presence of polygonized growth hillocks as observed in previous studies (cf. Paquette and Reeder, 1995). Individual calcite crystals were sectioned parallel to the $(10\bar{1}4)$ face of interest, with the as-grown surface exposed. Sections were mounted on high-purity silica glass disks. The resulting 30- to 50-μm-thick sections retained the growth microtopography, thereby allowing positioning of the incident light spot over different regions of the growth hillocks.

A selection of hand-picked single crystals were also ground to a fine powder for luminescence and EXAFS spectroscopy. Crystals were ground in acetone in a pestle and mortar and resulting powders were dried at room temperature. We refer to these as bulk calcite samples.

The high ionic strength of the solution used for growing the single crystals (method II) poses difficulties for simulation of the aqueous uranyl speciation. Ion activity coefficients determined using extended Debye-Huckel models are generally not accurate above ionic strengths of 0.5 mol/L. Reeder et al. (2001) simulated the aqueous uranyl speciation in two calcite growth solutions of ionic strengths 0.5 and 1.75 mol/L. For the I = 1.75 mol/L growth solution, which corresponds to the single crystals considered here, Reeder et al. (2001) used the Pitzer formulation as adapted by Felmy and co-workers in the program GMIN (Felmy, 1995; Felmy and Rai, 1999). However, interaction parameters for the $Ca_2UO_2(CO_3)_3(aq)$ species were not available for this simulation; hence this species was excluded, with the result that the $UO_2(CO_3)_3^{4-}(aq)$ species was predicted to account for > 98% of the aqueous U(VI). Kalmykov and Choppin (2000), however, experimentally determined the $Ca_2UO_2(CO_3)_3(aq)$/$UO_2(CO_3)_3^{4-}(aq)$ molar ratio over the ionic strength range 0.1 to 3.0 mol/L. Interpolating their results for I = 1.75 mol/L, we calculate that the molar ratio in the growth solution is ~25.3. Hence the $Ca_2UO_2(CO_3)_3(aq)$ species dominates over the $UO_2(CO_3)_3^{4-}(aq)$ species by an order of magnitude in this growth solution. As a further addendum to Reeder et al. (2001), we note that their simulation for the I = 0.5 mol/L solution accounted for the neutral $Ca_2UO_2(CO_3)_3(aq)$ species using the stability constant proposed by Bernhard et al. (1996) (log β_{213} = 26.8, I = 0 mol/L), with activity coefficients of charged species calculated using the Davies equation. Subsequently, Kalmykov and Choppin (2000) and Bernhard et al. (2001) have reported stability constants of log β_{213} = 29.8 and log β_{213} = 30.55 (both I = 0 mol/L), respectively, for the $Ca_2UO_2(CO_3)_3(aq)$ species. Despite uncertainty about a suitable activity coefficient for this neutral species, these larger stability constants make it likely that the $Ca_2UO_2(CO_3)_3(aq)$ species dominates over the $UO_2(CO_3)_3^{4-}(aq)$ species, which was previously predicted to dominate in the 0.5 mol/L growth solution.

3.2. Hyperspectral Fluorescence Imaging

Fluorescence spectra and images were acquired using a "push-broom" style microscopic imaging system based on a Carl Zeiss, Inc. Axiovert 135TV microscope, with the sample at room temperature. Samples were excited with ~1-mW vertically cylindrically focused 457.9-nm light from a Coherent, Inc. Innova400 Ar^+ laser which is delivered by a NA = 0.6 40x LD Achroplan objective. The resulting epifluorescence signal was collimated with the same objective and passed out of the microscope. Residual excitation light was removed with a Kaiser Supernotch holographic filter centered at the Ar^+ laser line. The fluorescence light was re-imaged on the 50-μm slit of a Kaiser Optical Systems Holospec f/2.2 spectrometer equipped with a broadband visible holographic transmission grating and imaged with a Roper Scientific LN_2-cooled CCD camera. Each 5-s integrated shot of the camera recorded frequency and y spatial information. X spatial information was acquired by stepping a Cell Robotics motorized sample stage. Frequency spectra were corrected to compensate for wavelength-dependent reflectivities of all components in the optical train using a white-light source as reference. Instrument control and data

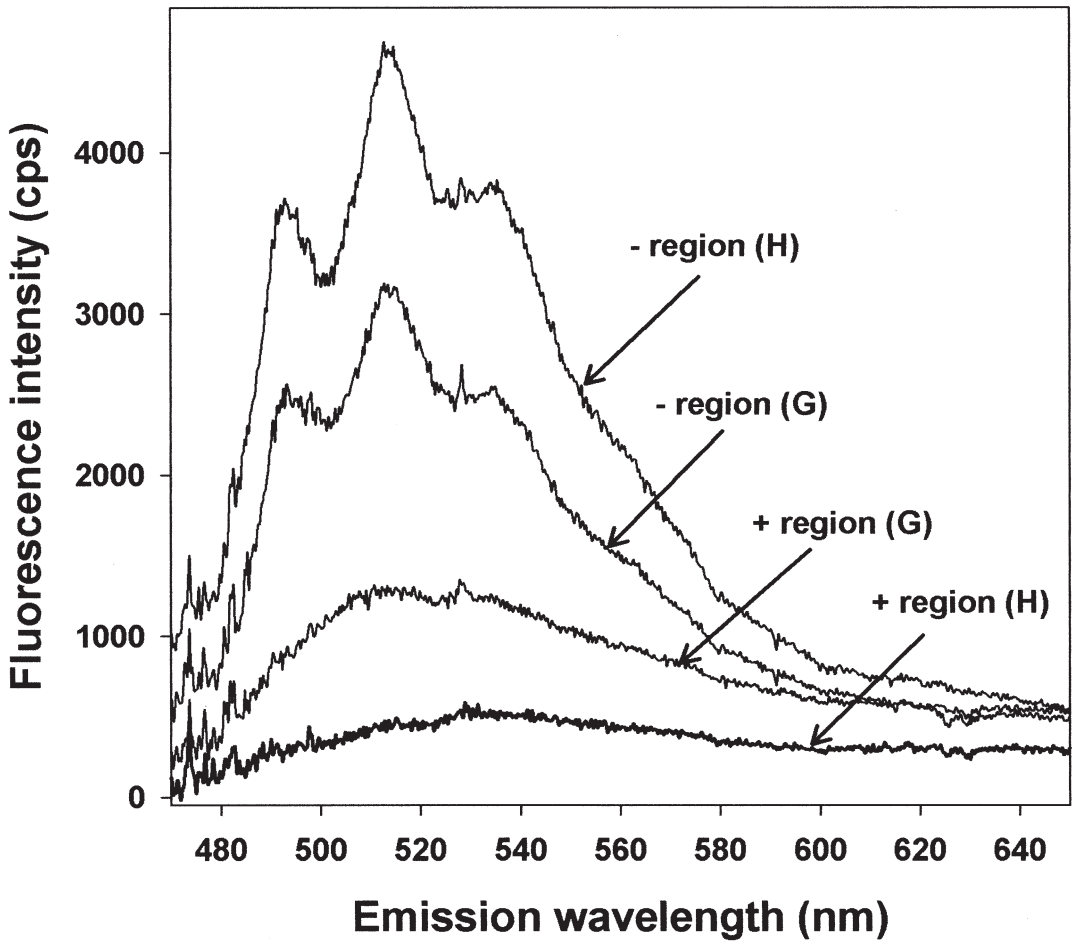

Fig. 2. Spatially resolved luminescence spectra obtained from the + and – vicinal regions of two U(VI)-containing calcite single crystals (crystals G and H) at room-temperature.

acquisition were performed using custom-written software routines.

4. RESULTS AND DISCUSSION

4.1. Hyperspectral Fluorescence Imaging of Uranium Distribution in Calcite

The fluorescence microscope was used to characterize the U(VI) present in the adjacent, non-equivalent vicinal regions of calcite single crystals that had been examined previously using μ-XRF, XANES, and luminescence (the latter in bulk samples only; Reeder et al., 2001). Room-temperature spectra for the + and – vicinal regions from two crystals are shown in Figure 2. The luminescence signal from the – vicinal regions is clearly more intense than that from the + regions (Fig. 2). While relative luminescence yields are not known, this difference in intensity is consistent with the higher concentration of U(VI) in the – region as documented by μ-XRF (Fig. 1). Peaks characteristic of uranyl are well-resolved in the spectra from U(VI) incorporated in the – vicinal regions, whereas spectral features from U(VI) in the + vicinal region are either strongly suppressed or absent. This suggests that not only does the concentration of incorporated U(VI) differ among the + and – regions, but that there are structural differences between the uranyl species incorporated in the + and – regions as well.

In Figure 3 the spatially resolved room temperature spectrum from the – region is compared with the low-temperature (~77 K) luminescence spectra of uranyl incorporated into calcite and aragonite (a metastable polymorph of $CaCO_3$) reported in previous studies (Reeder et al., 2000, 2001). As noted by Reeder et al. (2001) the spectrum of U(VI) incorporated into bulk calcite (i.e., multiple, powdered single crystals of the method II calcite) is red-shifted relative to the uranyl triscarbonate species observed in aragonite (Fig. 3). The uranyl spectrum from the method II calcite actually contained spectra from two species: the first having a spectrum identical to that found in aragonite and the second a shorter-lived species. The spectrum of this second species can be revealed most clearly by observing the luminescence spectrum from light emitted only at short times following the excitation flash. The spectrum for the uranyl-doped calcite synthesized differently (the method I calcite) is red-shifted even further relative to the method II calcite (Reeder et al., 2001) (Fig. 3). The uranyl species giving rise to all of these spectra were interpreted as based on uranyl triscarbonate-like species, ranging from a relatively undisturbed liebigite ($Ca_2UO_2[CO_3]_3$) structure for uranyl in arago-

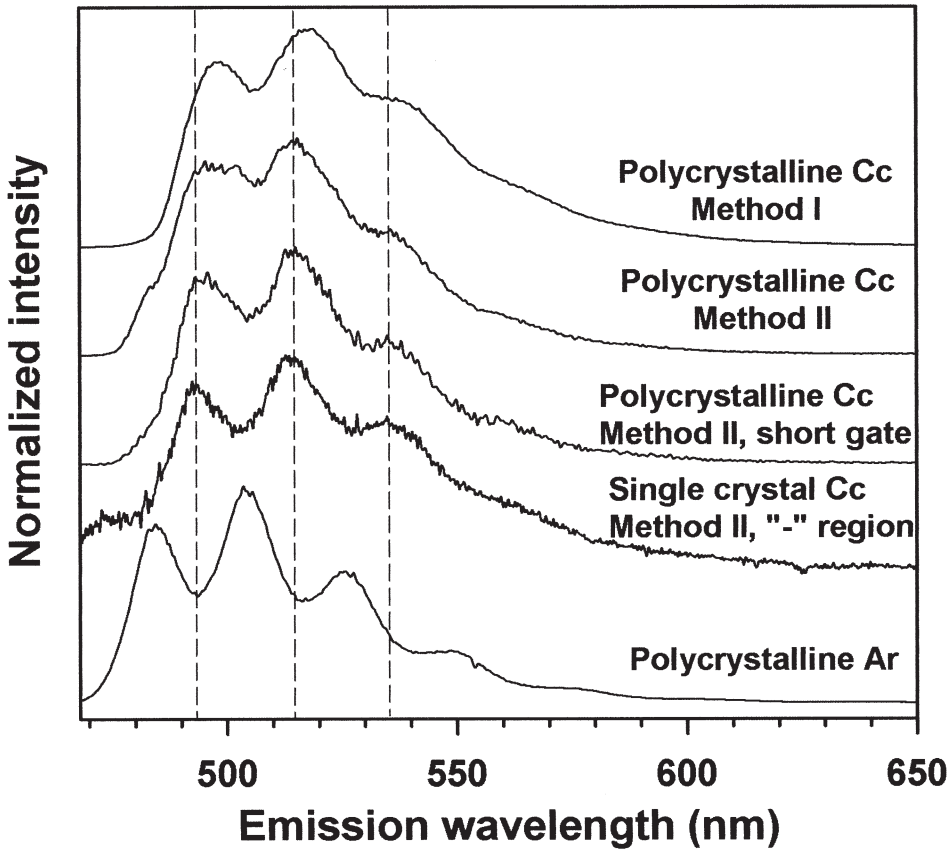

Fig. 3. Spatially resolved luminescence spectrum from the – vicinal region of a U(VI)-containing calcite single crystal (crystal G) compared with spectra obtained from bulk samples of U(VI) co-precipitated with polycrystalline aragonite and calcite (synthesized by two different methods). See text for explanation. Spectra from bulk samples taken from Reeder et al. (2001).

nite to a distorted local structure with bent and partially detached carbonate groups (five coordinate equatorial geometry) in method I calcite. The spatially resolved spectrum from the – vicinal regions closely matches the spectrum of the bulk method II sample, with only slight differences in the intensities of the secondary peaks (Fig. 3). This is expected inasmuch as the same material is used in each sample, the difference being only that the spatially resolved spectrum probes the U-rich vicinal region only whereas the bulk powder sample includes all regions of many similar crystals. It was not possible to determine decay kinetics for the single crystal luminescence, and hence our present results cannot confirm or rule out the presence of multiple species in the – vicinal region.

Because comparison of the spectrum from U(VI) incorporated in the + vicinal region is hindered by the lack of distinctive features, we have applied hyperspectral imaging to identify spatial-spectral differences. Figure 4 shows spatially resolved hyperspectral fluorescence imaging results obtained from a representative single-crystal calcite grown in a uranyl-containing solution. The background in Figure 4 is a bright-field image of the corner of a single calcite crystal containing adjacent non-equivalent vicinal surfaces labeled + and –. Overlaying the bright-field image are the results of a principal components analysis (PCA) from the hyperspectral fluorescence imaging in RGB false colors. Representative spectra from the two regions are shown in Figure 2 (Crystal G). The PCA procedure used to produce the RGB image will be described in a forthcoming communication. Briefly, the first three principal components, representing $> 98\%$ of the variance in the data, were generated using the PLS_toolbox software package from EigenVector Research (Manson, WA). The principal components targeted both the changes in shape and structure between the two spectra shown in Figure 2 for crystal G. Red, blue, and green regions were identified by large numbers of pixels with similar scores in two of the three principal components. There exists a sharp division between the red and blue groups corresponding to the + and – vicinal regions. The green group corresponds to "off crystal" signals. Pixels not falling into one of these groups are not colored and represent areas such as cracks, crystal defects, and crystal edges.

The RGB map shows that differences in the spectral signature coincide exactly with the non-equivalent vicinal regions. Micro-XRF had previously shown that these same regions have different U concentrations, resulting from differential incorporation. The present results demonstrate that there are differences in the local coordination environments of U(VI) incorporated in the + and – vicinal region as well. Such differences must be associated with processes at the non-equivalent steps associated with growth of the different vicinal regions, and hence imply a different mechanism for U(VI) burial in the +

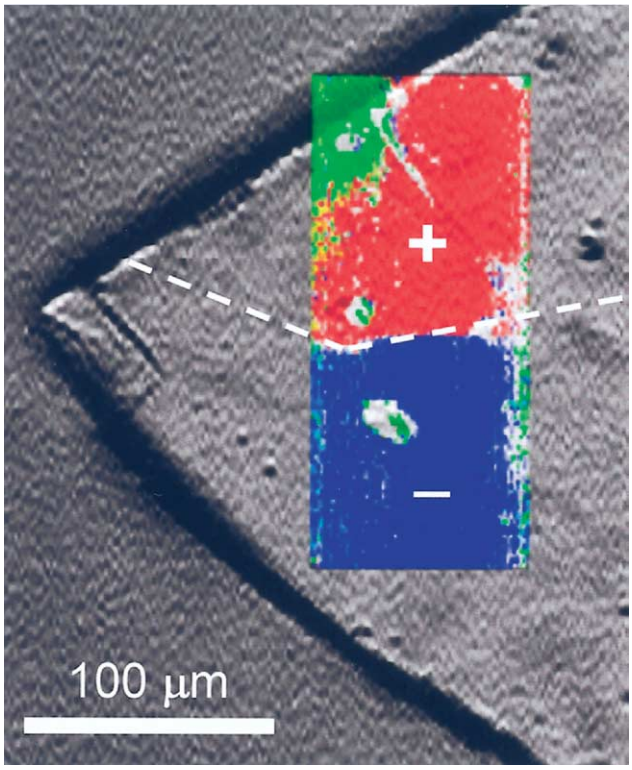

Fig. 4. Light microscope image of a portion of a U(VI)-containing calcite single crystal with an as-grown ($10\bar{1}4$) face exposed (background). Superimposed on the image is the result of a principal component analysis of spatially resolved hyperspectral images (see text for explanation). Different spectral components correspond with the + and – vicinal regions on the ($10\bar{1}4$) face.

and – growth steps. Uranium L_3-edge μ-XANES spectra reported by Reeder et al. (2001) failed to reveal any difference between the non-equivalent vicinal regions, suggesting that XANES is not sensitive to the differences that may exist.

We also used the confocal nature of the luminescence microscope to perform depth studies in the – vicinal region using spatially resolved luminescence imaging. This confirmed that the species responsible for the fluorescence is not limited to the surface alone. The luminescence is effectively collected from a spot measuring ~1 μm in the x, y dimensions and having a height of ~5 μm (z dimension corresponding to depth within crystal). The overall fluorescence intensity is sensitive to the probe depth within the crystal, although the shape and location of the peaks in the spectra are the same. The surface of the crystal was defined as the point at which the scattered light to the microscope eyepieces appears as the sharpest line focus. As the objective focuses the laser light deeper in the crystal, the fluorescence intensity increases by a factor of ~4 by 40 ± 1 μm into the crystal. Focusing deeper into the crystal beyond this point shows a monotonic decrease in fluorescence amplitude; by 120 ± 1 μm, the amplitude of the fluorescence has dropped back to the level that it was at the surface. As no corrections were performed to account for scattering, penetration, and other effects upon the depth profiling, these results should be considered qualitative, but suggest that the species is present in the crystal to a depth of at least 120 μm. The presence of the uranyl species to this depth is consistent with the synthesis procedure employed: steady-state growth of calcite single crystal seeds was achieved before addition of uranyl carbonate to the growth solution. Crystals were removed from the vessel 13 d after addition of U. A thickness of 120 μm of U-containing calcite yields an average linear growth rate of ~1 Å/s, which is consistent with previous growth rates reported using this method (Paquette and Reeder, 1995). Therefore, the U(VI) in these samples (which contributes to the observed luminescence and X-ray absorption signals) occurs as an impurity incorporated in the calcite overgrowth of a U-free seed.

4.2. Sorption Model for the Differential Incorporation of U(VI) Between Non-Equivalent Step-Edge Sites

The differential uptake of U(VI) between the + and – vicinal regions of the calcite ($10\bar{1}4$) growth surface is similar to the behavior exhibited by several other metal species and oxyanions showing distinct preferences for the different step types on this surface (e.g., Staudt et al., 1994; Paquette and Reeder, 1995; Reeder, 1996; Hemming et al., 1998). However, no unique step preference has emerged, and different metals and oxyanions exhibit preferences for different steps. Like U(VI), the oxyanions borate and arsenate also exhibit a preference for step edges associated with the – vicinals (Hemming et al., 1998). In contrast, sulfate and selenate exhibit a preference for step edges of the + vicinals (Staudt et al., 1994).

The finding by Elzinga et al. (2004) that the U(VI) sorption complexes at low coverage on calcite are calcium uranyl triscarbonate-like species, similar to the dominant aqueous species in the growth solution, allows us to propose a model for the preferential attachment of U(VI) species at the step edges on the – vicinal faces on the calcite ($10\bar{1}4$) growth surface. No structural difference occurs in the flat terrace portions within the non-equivalent vicinal surfaces; consequently, differences in uptake preference are interpreted to be related to the structure and coordination in step edges. The differences in structure between the + and – growth steps, both parallel to $<\bar{4}41>$, have been described in detail elsewhere (Staudt et al., 1994; Paquette and Reeder, 1995; Hemming et al., 1998). The most important distinction between the + and – steps is the orientation of CO_3 groups, which is controlled by bonding to Ca atoms and their positions (Fig. 5). In the bulk calcite structure, all CO_3 groups are co-planar. Exposed at the + steps, however, the CO_3 groups are oriented so that their leading edges are tilted down, toward the lower layer. In the – steps the orientation is opposite, with exposed edges of CO_3 groups tilted up and pointing away from the lower layer. In both steps, successive CO_3 groups along the step edge are alternately rotated 180° around the c-axis, but the fundamental distinction in their tilt direction remains the same.

In the $Ca_2UO_2(CO_3)$, unit, all CO_3 groups have bidentate linkage with the central uranium atom, resulting in three distal oxygen atoms, one from each group (Fig. 5 top). Each calcium atom also has linkages with two equatorial oxygen atoms from different carbonate ligands. The interaction of this uranyl species at either growth step should be controlled by coordination of the CO_3 ligand(s) and the Ca atom(s) in the equatorial plane of the complex with similar coordinating ligands exposed in the step edge. In particular, a CO_3 ligand of the complex is likely

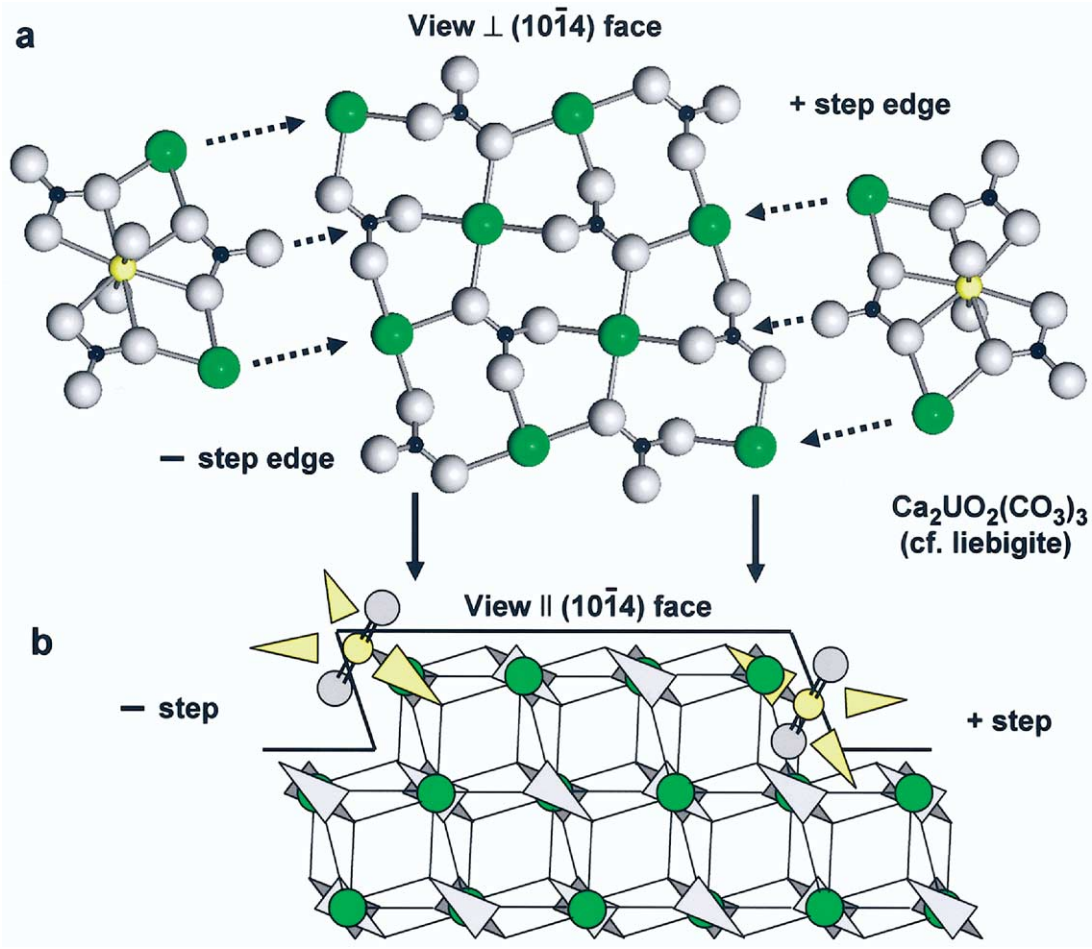

Fig. 5. (a) Structure model of a (10$\bar{1}$4) layer of calcite with edges corresponding to the four growth step orientations observed on spiral growth hillocks. $Ca_2UO_2(CO_3)_3$ species, as they occur in the liebigite structure (Mereiter, 1982) are shown in the orientations at each step type (+ and –) in which the bond topology is similar to that along the respective step. (b) View parallel to the (10$\bar{1}$4) growth face looking along growth steps of the + and – types. Here, the different tilt angles of the CO_3 groups (represented here as triangles) exposed at the different step edges are evident. If the orientation of sorbed $Ca_2UO_2(CO_3)_3$ species is controlled by the CO_3 tilt angle, so that it conforms with nearest-neighbor Ca positions, then adsorption of the species is seen to be hindered at + steps because of interference of an axial oxygen with layers below. Consequently, adsorption and subsequent incorporation are favored at – steps, which agrees with observed U(VI) distributions.

to coordinate at a step in a way that preserves the existing CO_3 tilt orientation in that step, as shown schematically in Figure 5 (bottom). This orientation is controlled by the positions of nearest Ca atoms. We note that the linkage between Ca atoms and CO_3 groups in the $Ca_2UO_2(CO_3)_3$ complex and that within the calcite structure at either step edge is topologically similar (Fig. 5 top), although in the latter structure Ca is not within the plane of the CO_3 group. In this model, we consider that this coordination (because of the topological similarities) forces the tilt of the $Ca_2UO_2(CO_3)_3$ complex to conform with the tilt existing at the corresponding step. It is worth noting that the alternation of CO_3 group *rotational* orientation (by 180°) suggests that every other site along a step edge is suitable for this coordination by a $Ca_2UO_2(CO_3)_3$ complex.

Figure 5 (bottom) illustrates the proposed orientations of $Ca_2UO_2(CO_3)_3$(aq) species coordinated in the + and – steps. If this model is correct, we see clearly that steric constraints favor coordination at the – steps and hinder coordination at the + steps. In the $Ca_2UO_2(CO_3)_3$ complex, the axial oxygens are oriented perpendicular to the CO_3 ligands within the equatorial plane. In the + step, the lower axial oxygen interferes with atoms in the lower layer. Assuming no relaxation, this configuration results in unrealistically short O-O_{ax} and Ca-O_{ax} distances of ~1.6 and ~1.3 Å, respectively. Consequently, we conclude that sorption of uranyl is sterically hindered in the + step.

In contrast, the tilt of the $Ca_2UO_2(CO_3)_3$ complex in the – step results in the lower axial oxygen being displaced away from neighboring oxygens, thereby allowing multidentate attachment at this step without steric hindrance. Therefore, we suggest that the $Ca_2UO_2(CO_3)_3$(aq) species interacts more favorably with the – steps, which should result in preferential incorporation in the associated – vicinal surfaces. This is in agreement with the observation of increased incorporation in the – steps.

Other geometries can be envisioned for coordination of a $Ca_2UO_2(CO_3)_3$ species, at both step and terrace sites. These are likely to be monodentate linkages, however, to avoid interac-

tion with the weakly reactive axial oxygens. Nevertheless, uranyl species sorbed in different coordination geometries are likely. Furthermore, our model does not preclude incorporation at the + steps despite the hindrance we describe, and the low but measurable U concentration in the + vicinal regions demonstrates some uranyl incorporation.

The luminescence results suggest that multiple uranyl species are present in the bulk calcite, and at least one of these species differs from the $Ca_2UO_2(CO_3)_3(aq)$ species. Our model describes the initial coordination at the steps associated with adsorption. Subsequent addition of Ca and CO_3 during growth eventually traps some of the sorbed uranyl, which gradually becomes buried within the bulk. In our model, it is unlikely that attaching Ca atoms and CO_3 groups could maintain ideal registry with the calcite structure and also complete the coordination around the incorporated uranyl species without local disruption or rearrangement, which is consistent with earlier reported EXAFS data of U(VI) incorporated into calcite showing a poorly ordered local coordination around U(VI) impurities (Reeder et al., 2000, 2001). Distortion of the geometry of the U(VI) adsorption species, including changes from bidentate to monodentate ligation with CO_3 groups, is possible during final entrapment. The EXAFS results reported earlier (Reeder et al., 2000, 2001) show that U(VI) incorporated into the calcite structure has a five-fold equatorial O shell, indicating a (partial) break-up of the exclusively bidentate coordination of CO_3 groups in the equatorial O shell of the triscarbonate complex as this species becomes incorporated.

Our findings suggest that the final coordination of uranyl incorporated into calcite depends on several factors associated with the reaction sequence encompassing initial adsorption through burial during growth. The distribution and availability of favorable binding sites at step edges are clearly important, and these may easily differ according to the synthesis method and details of the growth mechanism. The finding of a different coordination geometry of U(VI) in natural calcite by Kelly et al. (2003) also suggests that kinetic factors or aging effects could be important. Residence time of uranyl species at surface sites as well as the rate of Ca^{2+} and CO_3^{2-} addition during growth could also be influential. This may mean that multiple uranyl species should be expected to occur when co-precipitated with calcite.

5. CONCLUSIONS

This study characterizes the structural and compositional heterogeneity involved in U(VI) incorporation in the calcite $(10\bar{1}4)$ growth surface using spatially resolved luminescence spectroscopy. Incorporation of uranyl is strongly favored at the growth steps that compose the – vicinal surfaces of spiral growth hillocks, resulting in a heterogeneous distribution within the bulk crystal. Additionally, peaks characteristic of uranyl are well resolved in the luminescence spectra from U(VI) incorporated in the – vicinal regions, whereas spectral features from U(VI) in the + vicinal region are either strongly suppressed or absent, indicating a structural difference between U(VI) species incorporated in the + and – regions as well. The luminescence spectra from U(VI) in the – vicinal region match those observed for U(VI) in bulk samples, but differ slightly from spectra obtained from U(VI) co-precipitated with microcrystalline calcite via a different method, indicating that synthesis method and/or growth conditions affect the U(VI) incorporation mechanism. The preference for U(VI) incorporation at the – vicinal faces can be explained by preferred attachment of the calcium uranyl triscarbonate species at the step edges in the – region. The difference in atomic arrangement of carbonate groups at the + and – step edges results in much less steric hindrance during adsorption of the calcium uranyl triscarbonate complex at the – sites as compared to the + sites. Therefore, U(VI) adsorption is favored at the – steps, which may explain the observed preferred uptake of U(VI) in the – steps as compared to the + steps during crystal growth. The results of this study indicate that multiple uranyl species are to be expected when co-precipitated with calcite, and that the overall U(VI) speciation may vary with synthesis conditions and site availability.

Acknowledgments—Funding for RJR and EJE was provided by NSF grants CHE0221934 (Center for Environmental Molecular Science) and EAR0207756. Preliminary work contributing to this effort was supported by DOE grant DE-FG07-99ER15013. CDT and DEM were supported by the LANL Laboratory Directed Research and Development Program. We thank two anonymous reviewers for useful comments.

Associate editor: K. L. Nagy

REFERENCES

Bernhard G., Geipel G., Brendler V., and Nitsche H. (1996) Speciation of uranium in seepage waters of a mine tailing pile studied by time-resolved laser-induced fluorescence spectroscopy (TRLFS). *Radiochim. Acta* **74,** 87–91.

Bernhard G., Geipel G., Reich T., Brendler V., Amayri S., and Nitsche H. (2001) Uranyl(VI) carbonate complex formation. Validation of the $Ca_2UO_2(CO_3)_3(aq)$ species *Radiochim. Acta* **89,** 511–518.

Davis K., Dove P. M., and De Yoreo J. J. (2000) The role of Mg^{2+} as an impurity in calcite growth. *Science* **290,** 724–727.

Elzinga E. J. and Reeder R. J. (2002) X-ray absorption spectroscopy study of Cu^{2+} and Zn^{2+} adsorption complexes at the calcite surface. Implications for site-specific metal incorporation preferences during calcite crystal growth. *Geochim. Cosmochim. Acta* **66,** 3943–3954.

Elzinga E. J., Tait C. D., Reeder R. J., Rector K. D., Donohoe R. J., and Morris D. E. (2004) Spectroscopic investigation of U(VI) sorption at the calcite-water interface. *Geochim. Cosmochim. Acta* **68,** 2437–2448.

Felmy A. R. (1995) GMIN, a computerized chemical equilibrium program using a constrained minimization of the Gibbs free energy: Summary report. *Soil Sci. Soc. Am. Spec. Publ.* **42,** 377–407.

Felmy A. R. and Rai D. (1999) Application of Pitzer's equations for modeling the aqueous thermodynamics of actinides species in natural waters: A review. *J. Solut. Chem.* **28,** 533–553.

Gratz A. J., Hillner P. E., and Hansma P. K. (1993) Step dynamics and spiral growth on calcite. *Geochim. Cosmochim. Acta* **57,** 491–495.

Hemming N. G., Reeder R. J., and Hart S. R. (1998) Growth-step-selective incorporation of boron on the calcite surface. *Geochim. Cosmochim. Acta* **62,** 2961–2968.

Hudson E. A., Rehr J. J., and Bucher J. J. (1995) Multiple-scattering calculations of the uranium L_3-edge x-ray-absorption near-edge structure. *Phys. Rev. B* **52,** 13815–13826.

Hudson E. A., Allen P. G., Terminello L. J., Denecke M. A., and Reich T. (1996) Polarized x-ray absorption spectroscopy of the uranyl ion: Comparison of experiment and theory. *Phys. Rev. B* **54,** 156–164.

Kalmykov S. N. and Choppin G. R. (2000) Mixed Ca^{2+}/CO_3^{2-} complex formation at different ionic strengths. *Radiochim. Acta* **88,** 603–606.

Kelly S. D., Newville M. G., Cheng L., Kemner K. M., Sutton S. R., Fenter P., Sturchio N. C., and Spotl C. (2003) Uranyl incorporation in natural calcite. *Environ. Sci. Technol.* **37,** 1284–1287.

Mereiter K. (1982) The crystal structure of liebigite, $Ca_2UO_2(CO_3)_3(H_2O)_{11}$. *Tscherm. Mineral. Petrogr. Mitteil.* **30,** 277–288.

Paquette J. and Reeder R. J. (1995) Relationship between surface structure, growth mechanism, and trace element incorporation in calcite. *Geochim. Cosmochim. Acta* **59,** 735–749.

Reeder R. J. (1996) Interaction of divalent cobalt, zinc, cadmium, and barium with the calcite surface during layer growth. *Geochim. Cosmochim. Acta* **60,** 1543–1552.

Reeder R. J., Nugent M., Lamble G. M., Tait C. D., and Morris D. E. (2000) Uranyl incorporation into calcite and aragonite: XAFS and luminescence studies. *Environ. Sci. Technol.* **34,** 638 644.

Reeder R. J., Nugent M., Tait C. D., Morris D. E., Heald S. M., Beck K. M., Hess W. P., and Lanzirotti A. (2001) Coprecipitation of uranium (VI) with calcite: XAFS, micro-XAS, and luminescence characterization. *Geochim. Cosmochim. Acta* **65,** 3491–3503.

Staudt W. J., Reeder R. J., and Schoonen M. A. A. (1994) Surface structural controls on compositional zoning of SO_4^{2-} and SeO_4^{2-} in synthetic calcite single crystals. *Geochim. Cosmochim. Acta* **58,** 2087–2098.

Teng H. H., Dove P. M., and De Yoreo J. J. (1999) Reversed calcium carbonate morphologies induced by controlling microscopic growth kinetics: Insight into biomineralization. *Geochim. Cosmochim. Acta* **63,** 2507–2512.